# Rainfall Regime of a Mountainous Mediterranean Region: Statistical Analysis at Short Time Steps

Gilles Molinié, Davide Ceresetti, Sandrine Anquetin, Jean Dominique Creutin, Brice Boudevillain

# Rainfall Regime of a Mountainous Mediterranean Region: Statistical Analysis at Short Time Steps

GILLES MOLINIÉ, DAVIDE CERESETTI, SANDRINE ANQUETIN, JEAN DOMINIQUE CREUTIN, AND BRICE BOUDEVILLAIN

*LTHE, Université de Grenoble/CNRS, France*

(Manuscript received 11 January 2011, in final form 21 October 2011)

ABSTRACT

This paper presents an analysis of the rainfall regime of a Mediterranean mountainous region of southeastern France. The rainfall regime is studied on temporal scales from hourly to yearly using daily and hourly rain gauge data of 43 and 16 years, respectively. The domain is $200 \times 200$ km$^2$ with spatial resolution of hourly and daily rain gauges of about 8 and 5 km, respectively. On average, yearly rainfall increases from about 0.5 m yr$^{-1}$ in the large river plain close to the Mediterranean Sea to up to 2 m yr$^{-1}$ over the surrounding mountain ridges. The seasonal distribution is also uneven: one-third of the cumulative rainfall occurs during the autumn season and one-fourth during the spring. At finer time scales, rainfall is studied in terms of rain–no-rain intermittency and nonzero intensity. The monthly intermittency (proportion of dry days per month) and the daily intermittency (proportion of dry hours per day) is fairly well correlated with the relief. The higher the rain gauges are, the lower the monthly and daily intermittencies are. The hourly and daily rainfall intensities are analyzed in terms of seasonal variability, diurnal cycle, and spatial pattern. The difference between regular and heavy-rainfall event is depicted by using both central parameters and maximum values of intensity distributions. The relationship between rain gauge altitudes and rainfall intensity is grossly inverted relative to intermittency and is also far more complex. The spatial and temporal rainfall patterns depicted from rain gauge data are discussed in the light of known meteorological processes affecting the study region.

## 1. Introduction

The study region belongs to the Mediterranean part of France, which is historically prone to extreme precipitations and flash floods (Antoine et al. 2001). Should the climate change, this region could be one of the most affected in terms of extremes (Barnet et al. 2006; Giorgi 2006). In the recent past, a number of heavy rainfall events occurred: 144 events with daily precipitation amounts greater than 190 mm during the period 1958–1994 were inventoried by Jacq (1994), and 305 events with daily rainfall amounts greater than 150 mm during the 1967–2006 period are reported in Ricard et al. (2012). Each of the four more intense events of the last decade involved several tens of casualties and several billions of euros of damages (Jacq 1994; Sénési et al. 1996; Delrieu et al. 2005).

On the basis of the daily rainfall amount, Nuissier et al. (2011) analyze the synoptic circulations associated with heavy precipitation events (HPEs). They find out very similar patterns of atmospheric state variables like geopotential height at 500 hPa, wet-bulb temperature, or horizontal wind at 925 hPa. They also show that only small changes in these synoptic fields modify the intensity of HPEs from above the 99% quantile to above the 99.9% quantile. It is intriguing that such similar atmospheric conditions lead to rainfall with very different consequences. This suggests that local processes like flow–relief interaction could be at work, amplifying the rainfall production in some specific situations. Some processes of this kind have been revealed in Rotunno and Houze (2007) for example. In the study region, flow–relief interactions are obvious in banded orographic convection (Yates 2006; Anquetin et al. 2006; Godart et al. 2009), in deep organized convection (Nuissier et al. 2008; Ducrocq et al. 2008), and in combined situations (Ricard 2002). If the flow–relief interaction plays a significant role, it should be present both in the regular and heavy rainfall situations.

Previous research indicates that a potential climatological relationship between the rainfall and the topography depends on the temporal scale of analysis. At the

*Corresponding author address:* Gilles Molinié, LTHE BP 53, 38041 Grenoble, France.
E-mail: gilles.molinie@ujf-grenoble.fr

DOI: 10.1175/2011JAMC2691.1

daily time scale or longer, a rainfall–relief relationship seems to exist. The rainfall climatology of Alpine regions of Frei and Schär (1998) locates the highest annual and seasonal rainfall depth above the mountain ranges. At the event time scale, Alpert (1986), over the Judean Mountains in Israel, Michaud et al. (1995) over the southwestern Arizona and Colorado Plateau (United States), or Johnson and Hanson (1995) over the Reynolds Creek watershed (Idaho, United States) report good correlations between rainfall amounts and terrain elevation. At shorter durations, the correlation decreases, revealing the complexity of the rainfall–relief relationship (Johnson and Hanson 1995; Alpert and Shafir 1989, among others). In the region of interest, the link between extreme rainfall and the topography also appears to be very dependent on the temporal scales (Ceresetti et al. 2012, 2010). Extreme daily rainfalls are the highest over the relief, while extreme hourly rainfalls are the highest over the plain. Capitalizing both on the above knowledge of the hydrometeorology of the study region and on a reasonably long rain gauge dataset, this paper investigates the regional rainfall regime. This climatological study includes regular and extreme rainfall, covers a wide range of temporal scales from the hour to the year, and tries to establish links between the derived statistical regularities and known meteorological processes.

Section 2 describes the study region, the available rain gauge dataset, and the rainfall event selection. Point rainfall accumulation is analyzed in section 3. This section depicts both the annual rainfall depth pattern and its seasonal variability, which are key factors for water resources. Then the analysis is conducted at shortest time steps: daily and hourly. In section 4, rainfall is characterized by its rain–no-rain intermittency and intrinsic intensity. Section 5 is dedicated to space and time rainfall patterns. Namely, first the diurnal cycle of the rainfall intensity is analyzed, then the rainfall intensity spatial pattern. Section 6 is dedicated to extreme rainfall at the daily and hourly temporal scales. Section 7 provides a cross analysis of the rainfall statistics of the regular and extreme rainfall is performed at the hourly and daily scales to identify signatures of meteorological processes in the observed rainfall patterns. Section 8 recalls the main results of this study and discusses the use of rain gauge data.

## 2. Context

### a. The physical region

The study region is located in the southeast of France and roughly covers $200 \times 200$ km$^2$ (Fig. 1a). The Rhône River flows across this area between two major mountainous massifs: the Hercinian V-shaped Massif Central at the west and the Tertiary orogenic belt of the Alps at the east. The eastern side of the Massif Central facing the Rhône River valley is oriented 30° clockwise from the north and is strewn with several mounts such as Mont Aigoual (1565 m height above mean sea level, i.e., MSL), Mont Lozère (1699 m MSL), Mont Gerbier de Jonc (1551 m MSL), and Mont Mezenc (1753 m MSL) forming the Cévennes–Vivarais region. On the eastern side of the study domain, the Alps foothills forming the Baronnies region are almost as high as the Massif Central Ridge. The northwestern quarter of the region is a quite homogeneous high plateau. The southern part of the region is a large river plain. The Mediterranean Sea shore constitutes the south border of the study region.

Because the western part of this region (Cévennes–Vivarais) is very sensitive to flash-flood events (see section 1), an enhanced survey of hydrometeorological parameters is in operation since 2000 and managed by the Observatoire Hydro-météorologique Méditerranéen Cévennes–Vivarais (OHMCV; Delrieu 2003). The region is covered by three meteorological S-band radars with specific scanning protocols as well as by dense hourly and daily rain gauge and river-discharge networks. OHMCV favored a synergy between hydrologists and meteorologists through modeling and data analysis studies, so that the region has been chosen as a focus site for the Hydrological Cycle of the Mediterranean Experiment (HyMEx; http://www.hymex.org).

### b. Available rainfall data

This study relies on two rainfall databases collected by the French meteorological service Météo-France: (i) daily rainfall records from 1958 to 2000 and (ii) hourly records from 1993 to 2008. The daily and hourly rain gauge networks are displayed in Fig. 1b. The rain gauges are distributed quite homogeneously in the study area. It is obvious from Fig. 1b that the daily network is denser than the hourly one. For the entire study period, the average distance between neighbor rain gauges increases from 5 km to about 8 km when considering, respectively, the daily and the hourly databases. The rain gauge density varies with the altitude. The daily (hourly) rain gauge density increases from 3.5 (100 km$^2$)$^{-1}$ [1.4 (100 km$^2$)$^{-1}$] in the 0–500-m altitude range to 28 (100 km$^2$)$^{-1}$ [5 (100 km$^2$)$^{-1}$] for the area where the altitude is higher than 900 m. This atypical density repartition illustrates the care taken by Météo-France and the involved water agencies to survey mountainous rainfall. The rain gauge availability depends also on date. The number of daily rain gauges has increased from 280 in 1958 to about 380 since 2000. The number of hourly rain gauges was about 50 in 1993 and increased to 320 in 2008. This kind of heterogeneity is very common given the evolution of the measurement devices and the network management constraints. To avoid complex combination of the datasets we simply

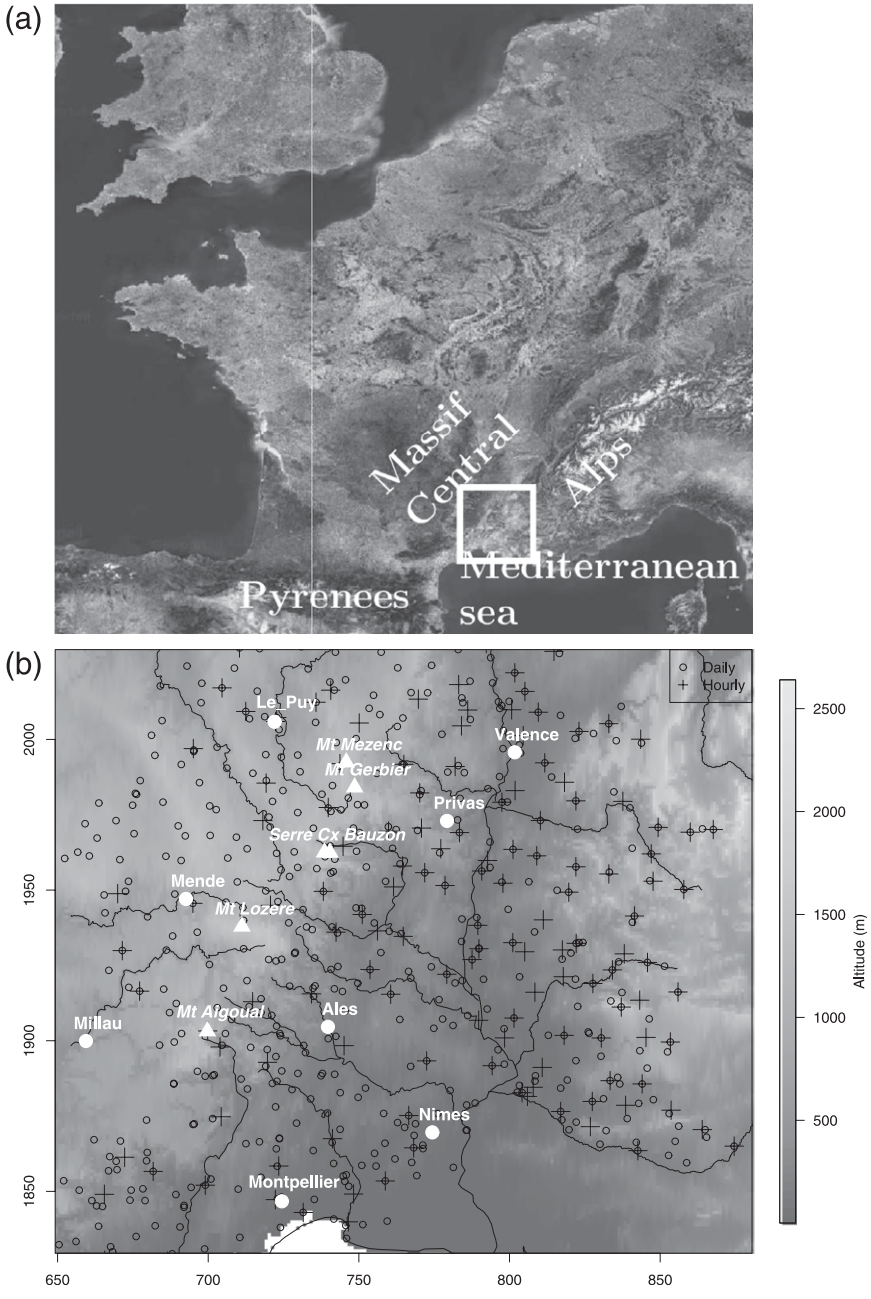


FIG. 1. (a) Physiographic map of France (western Europe). The study region is outlined by a white rectangle in the southeast. (b) Close-up of the study region. The terrain elevation is displayed as a gray-shaded surface. The white circles and triangles point out, respectively, the main towns and mountain peaks. The solid lines display the hydrographic network. The open circles indicate the locations of daily rain gauges; crosses indicate the hourly ones.

decided to use the two networks as such. The daily network has been used to characterize rainfall accumulations over time steps ranging from one day to one year as well as to study the so-called daily intensities. The hourly network served to study hourly rainfall intensity and intermittency. All the daily rain gauges (hourly) are synchronized. A daily record integrates rainfall from 0600 to 0700 UTC next day.

### c. *Rainfall event selection*

For the analysis of intensity and intermittency, we decided to ignore very light events and restrict focus to

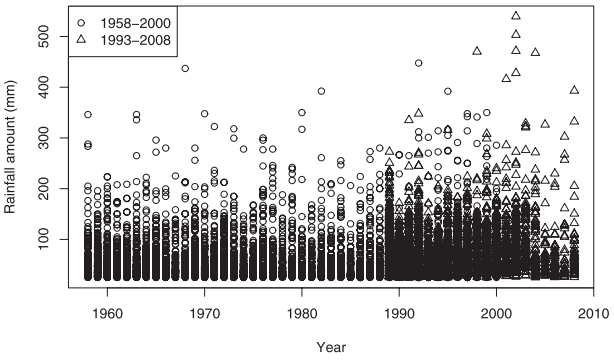


FIG. 2. Maximum point daily rainfall depth during rainfall events.

moderate to heavy events. According to a definition proposed by Météo-France, a rainy event is a day (0600–0600 UTC) during which at least one rain gauge of the study area records a rain amount larger than 25 mm (the 50th percentile of the nonzero daily rainfall amounts). According to the academic definition of an event, the definition proposed by Météo-France may appear restrictive because rainy periods may last several consecutive days. Nevertheless as long as no event statistics are specifically needed, such a selection is operative in terms of light rain filter. For internal coherence reasons, we performed the event selection on the two databases independently. In particular, daily accumulations of hourly records have been used to select the rainy events from the hourly database. To illustrate the coherence of these two databases, the maximum rainfall amounts per event are displayed over the period 1958–2008 in Fig. 2. This figure shows that during the 1993–2000 overlapping period, the maximum rainfall amounts recorded during the events selected from the hourly database are of the same order of magnitude and of about the same evolution than those selected using the 1958–2000 database. Obviously, there is not an exact match between the maximum amounts recorded by the two databases, as rain gauges of the two networks are not collocated. After 2000, the order of magnitude and the evolution of the maximum rain amounts are similar to these of the daily database, even though the exceptional 2002 Gard event (Delrieu et al. 2005), featuring a return period of 500 yr, could imply the impression of a bias in the event selection using the aggregated hourly database.

## 3. Point rainfall accumulation

### *a. Annual rainfall accumulation*

The mean annual rainfall accumulation over the 1958–2000 period was 667 mm with a standard deviation of 388 mm. The gross partition of the rainfall accumulation as a function of rain gauge altitudes shows a monotonic increase (Table 1). The spatial distribution of the mean annual rainfall accumulation is mapped in Fig. 3a. The map is obtained by kriging rainfall accumulations at rain gauge stations [see appendix B and Chiles and Delfiner (1999)]. The mean rainfall accumulation is minimum in the Rhône River valley and increases gradually over the western Alpine foothills (Baronnies) and the eastern slope of the Massif Central (Cévennes–Vivarais). We notice that the highest of the mean annual accumulations are double over the Cévennes–Vivarais Mountains than over the Baronnies hills. The maximum rainfall gradient is very well correlated with the slope in particular over the Cévennes–Vivarais Range. The maximum annual rainfall accumulation of 3521 mm has been recorded at the station of Mont Aigoual in 1996 (see Fig. 1b to locate Mont Aigoual and other mounts refereed in the following). This station, at the south of the Cévennes Ridge, records also the highest mean annual accumulation (2157 mm). However, as it can be seen in Fig. 3a, the Mont Aigoual station (1567-m altitude) is far from the maximum of the kriged mean annual accumulation located around the Serre de la Croix de Bauzon massif (1538 m), north to the highest mountain of the chain (the Mont Lozere, 1699 m). In this subregion, the station of Loubaresse (1220-m altitude) has recorded the second highest mean annual accumulation (2149 mm) and 4 out of the 5 highest are also around. The relative variability (coefficient of variation, ratio of the standard deviation to the mean) of the annual rainfall accumulation is the lowest in the plain region (Fig. 3b). Its gradient is roughly directed toward the northwest where the annual rainfall relative variability is the highest. An area of low variability remains around Mont Aigoual and Alès even though in this region the altitudes strongly vary (Alès, 135-m altitude; Mont Aigoual, 1567 m).

TABLE 1. Mean rainfall accumulation between 1958 and 2000 in given altitude ranges.

| Alt range (m) | 0–200 | 200–500 | >500–900 | >900 |
|---|---|---|---|---|
| Rainfall amount (mm) | 811 | 1064 | 1111 | 1137 |

The altitude obviously influences the annual rainfall accumulation. Nevertheless, the high rainfall amounts around Serre de la Croix de Bauzon indicate that other factors may interact at this place particularly and possibly at other ones.

### *b. Seasonal variability*

The seasonal cycle of monthly rainfall amounts displays two maxima (Fig. 4). The highest one occurs roughly during the fall season (September, October, and November), and the smaller one during the spring (from April to

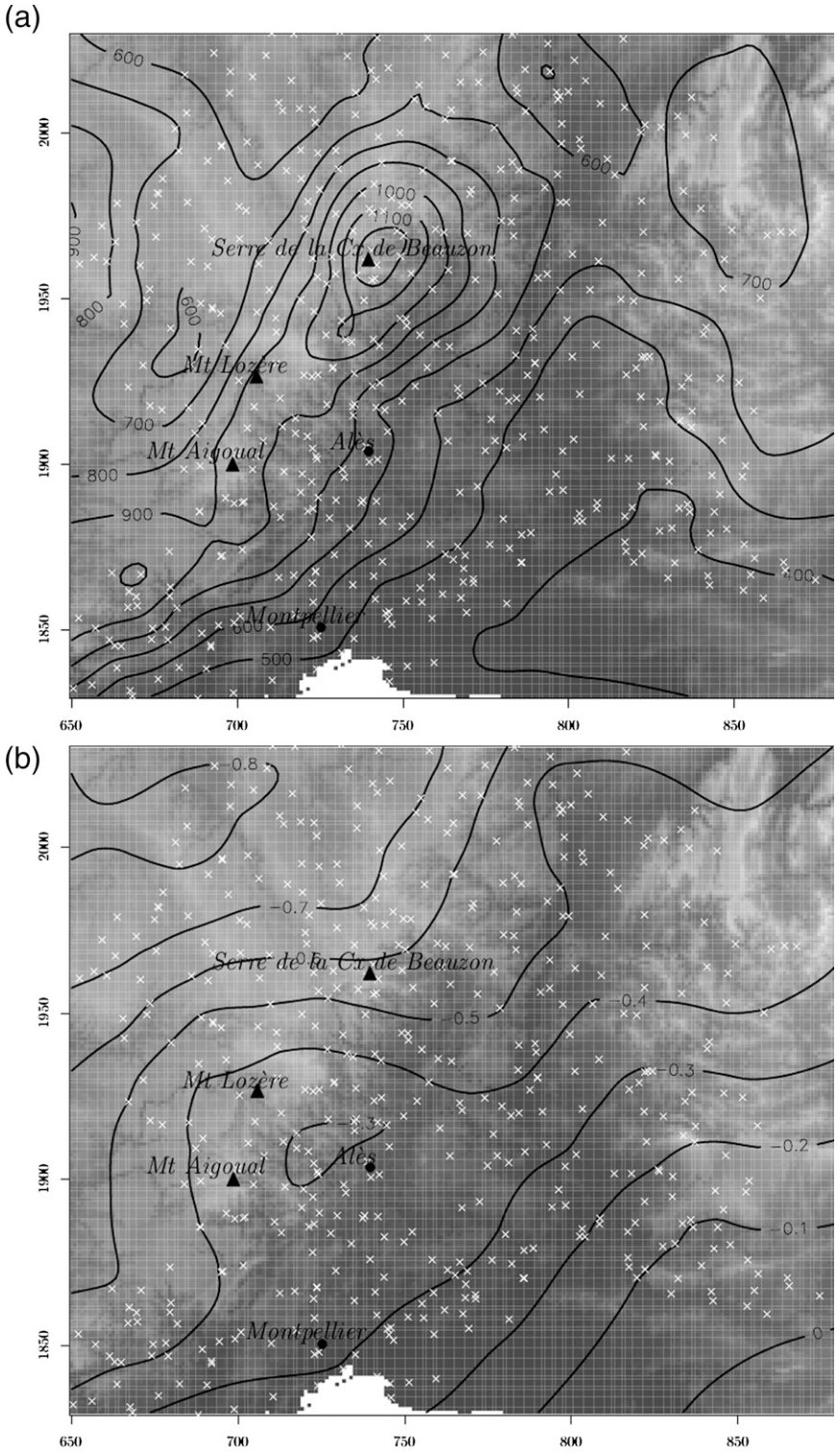


FIG. 3. (a) Mean annual rainfall accumulation for the 1958–2000 period. Computed from the daily database and kriged using a spherical variogram model (nugget = $1.1 \times 10^5$ mm$^2$; range = 76 km; sill = $1.6 \times 10^5$ mm$^2$). (b) Coefficient of variation of the annual rainfall amount (variogram for kriging: nugget = 0.65; range = 92 km; sill = 0.68). The white crosses indicate the locations of daily rain gauges that were used to compute the isolevels.

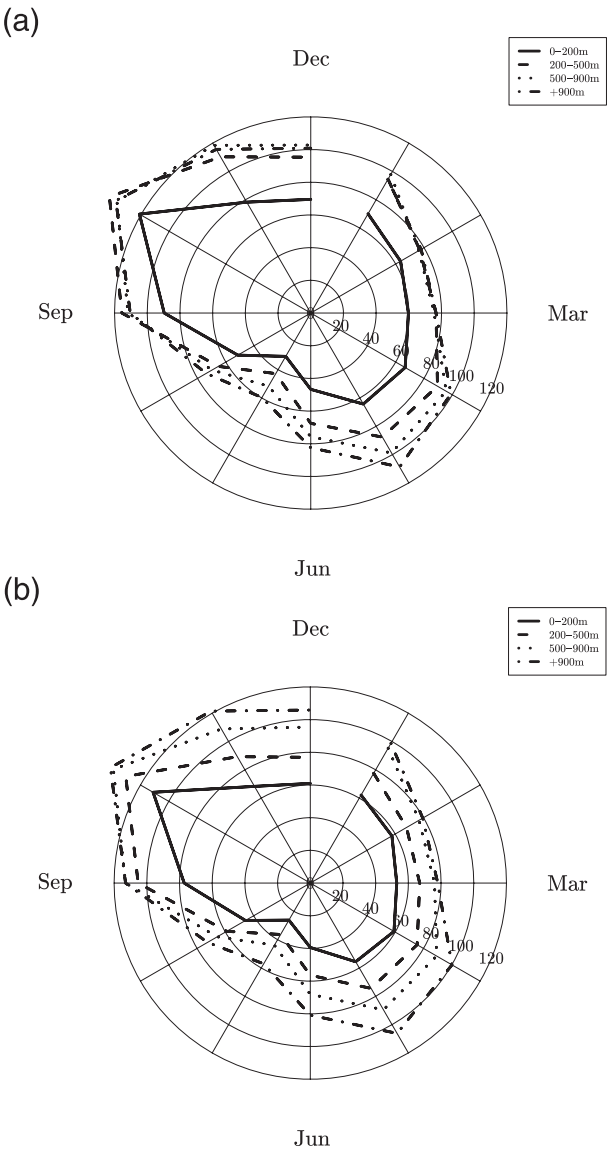


FIG. 4. Annual cycle of the monthly rainfall amounts (mm) averaged over 42 yr in four altitude ranges (m): 0–200 (solid black), >200–500 (dashed), >500–900 (dotted), and >900 (dashed–dotted). (a) Rain gauge altitudes are the original ones. (b) Rain gauges altitudes are set to the 90th percentile of the terrain elevation in a radius of 5 km around each rain gauge.

June). The average of the cumulative rainfall depth during the fall is of 226 mm, one-third of the annual amount against one-fourth for the spring season (157 mm).

Figure 4a shows the seasonal cycle of the monthly rainfall accumulation for rain gauges at different altitudes. In this figure, the relationship between rainfall accumulations and rain gauge altitudes presents a more complicated behavior than the monotonic trend of the annual rainfall accumulations (Fig. 3a). These differences are either due to a seasonal component in the rainfall regime or to an artifact due to the rain gauge altitude, or both. Assuming a positive correlation between terrain elevation and rainfall accumulation, an artifact clearly appears at least in the region of the Serre de la Croix de Bauzon (Fig. 1b). Since the rain gauges are located in a narrow valley, their altitude is not representative of the surrounded relief. The rain gauge altitudes are between 480 and 600 m while the surrounding relief reaches more than 1500 m in height. To check this hypothesis, the rain gauge altitudes have been replaced by the 90th percentiles of the relief altitude in a 5-km radius around the rain gauges (empirical correction). Fig. 5 shows histograms of the rain gauge altitudes before and after this adjustment. We see an increase in the number of stations in the altitude ranges of 500–900 and >900 m versus a decrease of the number of stations below 500 m. In the polar plot of the monthly rainfall accumulation including the altitude correction (Fig. 4b), the rainfall–rain gauge altitude relationship is more monotonic; at any period of the year, the rainfall accumulation increases with the altitude. The comparison between Figs. 4a and 4b shows that the rain gauge altitude adjustment has the largest effect during the fall. The rainfall accumulation over 500 m MSL has specifically increased while it decreases below 200 m MSL. This highlights the occurrence of a specific rainfall regime during the fall and in mountainous area, in particular around the Serre de la Croix de Bauzon area. This is further discussed in the light of some meteorological processes in section 7.

## 4. Intermittency and intensity

Over a given period of time and given a time step of analysis, the rainfall accumulation depends both on the rainfall intermittency (percentage of nonrainy time steps) and on the average nonzero rainfall intensity (rainfall accumulation per time step that we simply name as intensity hereinafter). The accumulation turns out to be the product of these two terms multiplied by the number of time steps in the period. These two properties of the rainfall series (or fields) are dependent on the scale of analysis (e.g., Barancourt et al. 1992; Braud et al. 1993; de Montera et al. 2009; Molini et al. 2010).

### *a. Rainfall intermittency*

The intermittency is the proportion of dry weather over a given period. On one hand, we consider periods of one month at the daily resolution. This leads to the so-called monthly intermittency (i.e., the proportion of dry days per month). On the other hand, the intermittency is studied for periods of one event (one day) at the hourly resolution. It is called the event intermittency and measures the proportion of dry hours per event.

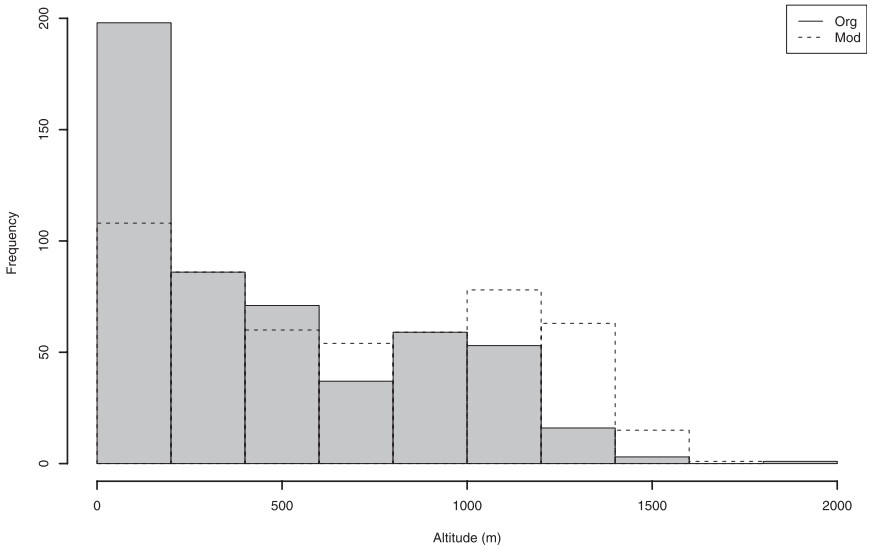


FIG. 5. Histograms of the rain gauge altitudes. The shaded boxes indicate the original rain gauge altitudes; the dashed lines indicate the rain gauge altitudes set to the 90th percentile of the terrain elevation in a radius of 5 km around each rain gauge.

Practically, a period of dry weather is a period during which the rainfall intensity is lower than the detection threshold of the measurement device. In this study, rain gauges have a resolution of 0.1 mm.

In addition, the rain gauge altitude adjustment described in the previous section has been applied.

Figure 6a displays the event intermittency averaged for each month and altitude ranges similar to those of section 3b. The event intermittency shows a monotonic decrease with altitude, meaning that the higher the rain gauge altitude, the higher is the rainfall frequency during a rainy event. From December to April, the event intermittency is in between 0.85 and 0.98 depending on the altitude range. This means that during rainy events, the average number of rainy hours is of 3.5 h above 900-m altitude and less than 2 h below. From April to September, the number of rainy hours during rainy events still decreases to about 2 and 1 h in July and August. In September, October, and November, the intermittency decreases dramatically. In November, there is an average of more than 3.5 h rainy hours during rainy events and even about 4.8 h above 900 m MSL. The station-to-station and interannual variability of the event intermittency is relatively low, less than 10%, except in November where it reaches 30% (not shown).

The average of the monthly intermittency (Fig. 6b) is quasi-symmetric relative to the January–July axis. At the lowest altitudes, the intermittency is about the same during the fall and the spring (about 7.5 wet days per month), it is the highest during the summer (~3 wet days per month) and the lowest during the winter (~9 wet days per month). On average the intermittency decreases with the altitude in a monotonic way. The number of wet days per month reaches 7.5 above 900-m altitude during the summer, 13 in September, and up to 15 during the winter. The monthly variability of intermittency from station to station is relatively low, below 10%. It is the most variable at the highest altitudes. During July and below 200-m elevation, the intermittency is the least variable (less than 4% of the mean intermittency) and the highest. According to climate classification systems such as the Köppen one (Pidwirny 2011; Peel et al. 2007), dry summers and wet winters are among the criteria to identify a Mediterranean climate. These features are mainly due to synoptic forcing, that is, the Azores high pressure system (Bolle 2003).

Both the rainfall amount and intermittency suggest that rainfall intensity data can be grouped in four 3-month clusters that are close to the actual seasons: winter (December, January, and February), spring (March, April, and May), summer (June, July, and August), and fall (September, October, and November). For these clusters, the monthly intermittency is computed at each station, kriged [see appendix B and Chiles and Delfiner (1999)], and mapped. We only report here the monthly intermittency for the fall season (Fig. 7) as the patterns are similar for the other seasons. Table 2 gives the parameters of the fitted variograms [appendix A and Chiles and Delfiner (1999)]. The variogram model parameters result from, first, a least squares fit of a spherical model on the empirical variogram, and second, a heuristic correction

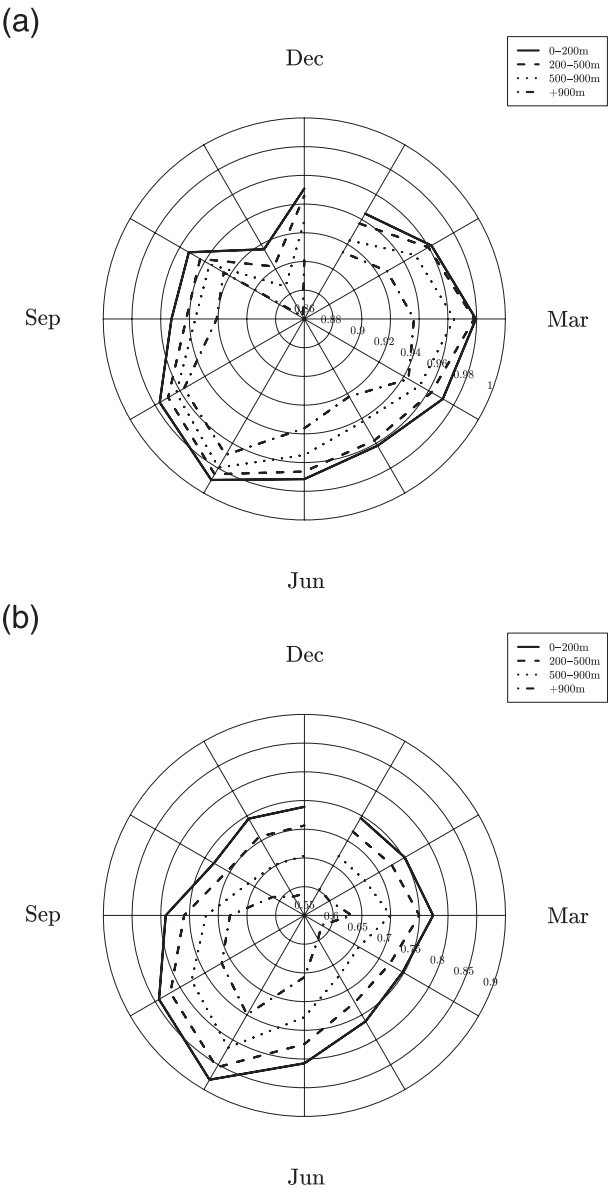


FIG. 6. Precipitation (a) seasonal cycle and (b) monthly intermittency.

to avoid the overestimation of the nugget effect as shown in Lebel and Bastin (1985) (appendix A explains variogram features). The nugget effect is due to the local variability of the analyzed variable. Table 2 indicates that the local variability of the monthly intermittency is very high, at least two-thirds of the sill. It is the highest during the fall and the lowest in the summer. In addition, the variogram sill is lower in the summer than during the other seasons. This indicates that variability of the intermittency is the lowest during the summer. The gradient of the monthly intermittency is parallel to the main mountain slopes (Cévennes–Vivarais and Baronnies) thus forming a thalweg along the Rhône River valley.

### *b. Intrinsic-rainfall intensity*

The rainfall intensity is the ratio of the rainfall accumulated over a given period to this period length. As stated before, we consider only the nonzero rainfall intensities corresponding to selected rainfall events. They are computed in the following for periods of 1 h (hourly intensity) and of 1 day (daily intensity).

To analyze the seasonal variability, the intensities have been gathered by month and altitude range. As in section 3b, rain gauge stations are in four elevation range categories; 0–200, >200–500, >500–900, and >900 m. The seasonal evolution of the average and variation coefficient of the hourly intensity in the four altitude ranges are displayed in Fig. 8. The average hourly intensity is the lowest during the winter. It increases gradually during the spring to reach its maximum from July to October and then decreases again. The intensity–altitude relationship is opposite to the one of the monthly accumulation; that is, the average intensity decreases with the altitude. It is important to note that the variation coefficient (Fig. 8b) is very high at any month and especially during the summer where the standard deviation is 12 times the average intensity in the lowest elevation bin (0–200 m).

The seasonal evolution of daily intensities is displayed in Fig. 9a. As for the hourly time step, the seasonality of daily intensities is well marked. However, the hourly and daily seasonality patterns are different. The daily intensity is slightly bimodal with a main maximum during the fall and another minor one during the spring. In September and October the intensity average reaches its maximum of about 15 mm day$^{-1}$ (1.6 times the annual mean of 9 mm day$^{-1}$). The spring mode is well below with about 8 mm day$^{-1}$. The summer features the lowest daily rainfall intensities.

The relationship with the altitude is more complex than for hourly intensities. For the stations above 200 m MSL, the daily intensities monotonically decrease with altitude like the hourly intensities. However, for the stations below 200-m height (in the plain), the intensities are lower than expected from a monotonic relationship. Moreover during the month of July, the relative variability at these plain stations is particularly high compared to the other stations (Fig. 9b).

The comparison between Figs. 9a and 8a shows that in July the daily and hourly intensities over the plain (altitude < 200 m) are about the same (4 mm day$^{-1}$). The rainfall in plain during the early summer is thus due to storms lasting about one hour. For stations above 200-m altitude, the daily intensity is about 10 mm day$^{-1}$, at

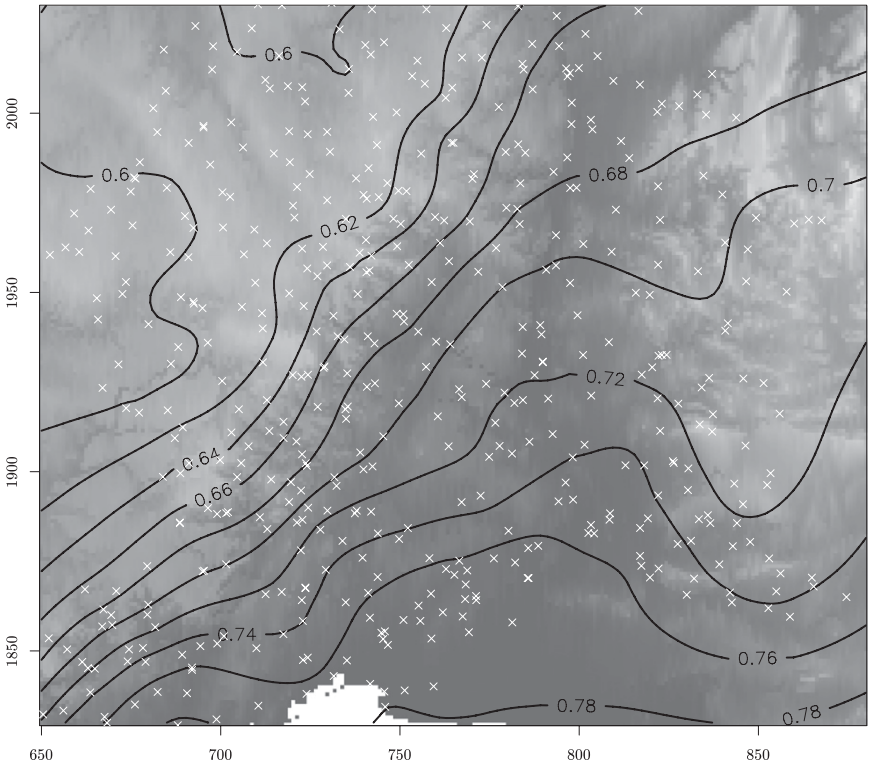


FIG. 7. Map of the monthly intermittency averaged over September, October, and November. The background topography is similar to Fig. 1b.

least 2 times the hourly intensity. From August to November (with a peak in September and October), the daily intensity is notably larger than the hourly one even if a large uncertainty is due to the hourly sampling (on average 40% according to ongoing investigations).

These differences between the hourly and daily intensities are further discussed in section 7.

## 5. Rainfall patterns in time and space

### a. Diurnal cycle

Another important feature of the rainfall regime is the diurnal cycle. The analysis of the rainfall intermittency having not shown any clear diurnal signature, we focus in this section on the intensity. In Fig. 10, the normalized rainfall intensity (divided by the average) is displayed as a function of the hour of occurrence for the four seasons considered in section 3a. During the winter, there is no diurnal cycle of the intensity. During the spring and summer, the intensity displays two peaks, one major at the end of the afternoon and another minor one in the early morning, before the sun set. In September–October, the rainfall-intensity diurnal cycle presents a different trend. It peaks during the night. Such a change indicates a modification of the atmospheric forcing mechanisms and of the synoptic environment of autumn rainfall in comparison to summer and spring ones (further discussed in section 7).

### b. Bulk spatial patterns

The variation coefficients of both hourly and daily intensities are high (Figs. 8 and 9), indicating the high rainfall variability at those space and time scales. The spatial features of the daily and hourly rainfall intensities allow for an assessment of their variability. Because of the long tails of rainfall intensity distributions (Ceresetti et al. 2010), the intensity average is significantly influenced by the highest values. Therefore, we analyze in this section medians of the daily and hourly intensities for two

TABLE 2. Parameters of the spherical variogram model fitted onto the experimental monthly intermittency variogram: $\gamma(h) = (s - n)\{[(3h/2r) - (h^3/2r^3)]1_{(0,r)}(h) + 1_{(r,\infty)}(h)\} + n1_{(0,\infty)}(h)$, where $1_{(a,b)}(x)$ is the indicator function that is equal to 1 if $x \in [a, b]$ and 0 otherwise.

| | Dec–Feb | Apr–Jun | Jul–Aug | Sep–Nov |
|---|---|---|---|---|
| Nugget effect $n$ | $2.58 \times 10^{-3}$ | $2.03 \times 10^{-3}$ | $1.38 \times 10^{-3}$ | $3.04 \times 10^{-3}$ |
| Sill $s$ | $3.72 \times 10^{-3}$ | $3.23 \times 10^{-3}$ | $1.98 \times 10^{-3}$ | $3.99 \times 10^{-3}$ |
| Range $r$ (km) | 51.5 | 61.9 | 111.4 | 117.1 |

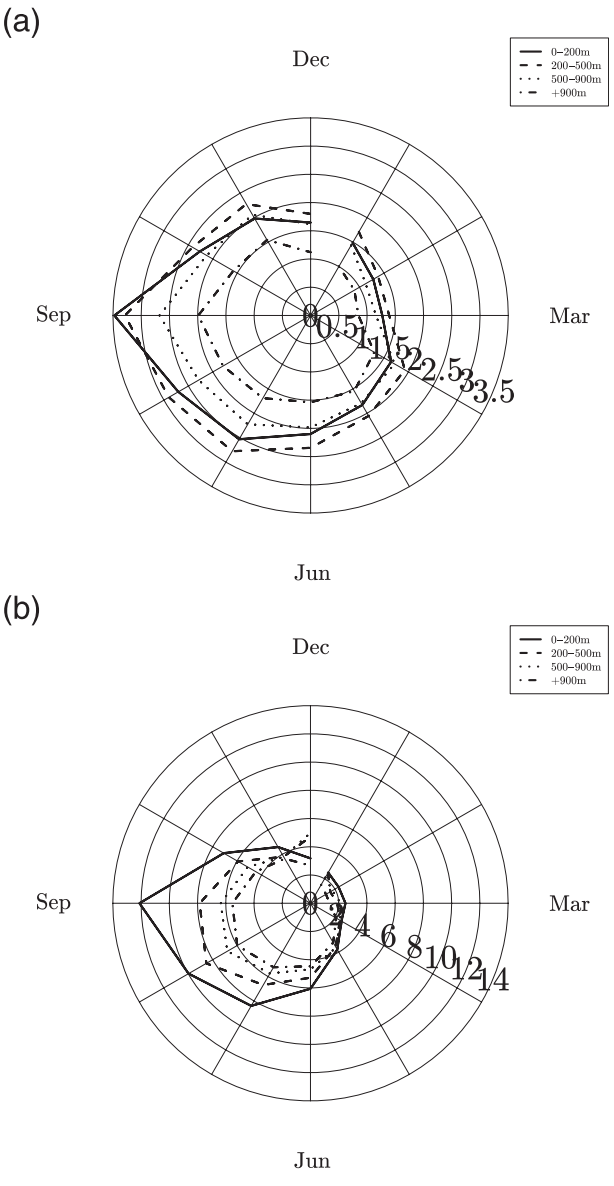


FIG. 8. Monthly average (a) and coefficient of variation (b) of the hourly intrinsic-rainfall intensity (mm $h^{-1}$) in four altitude ranges (0–200, >200–500, >500–900, and >900 m).

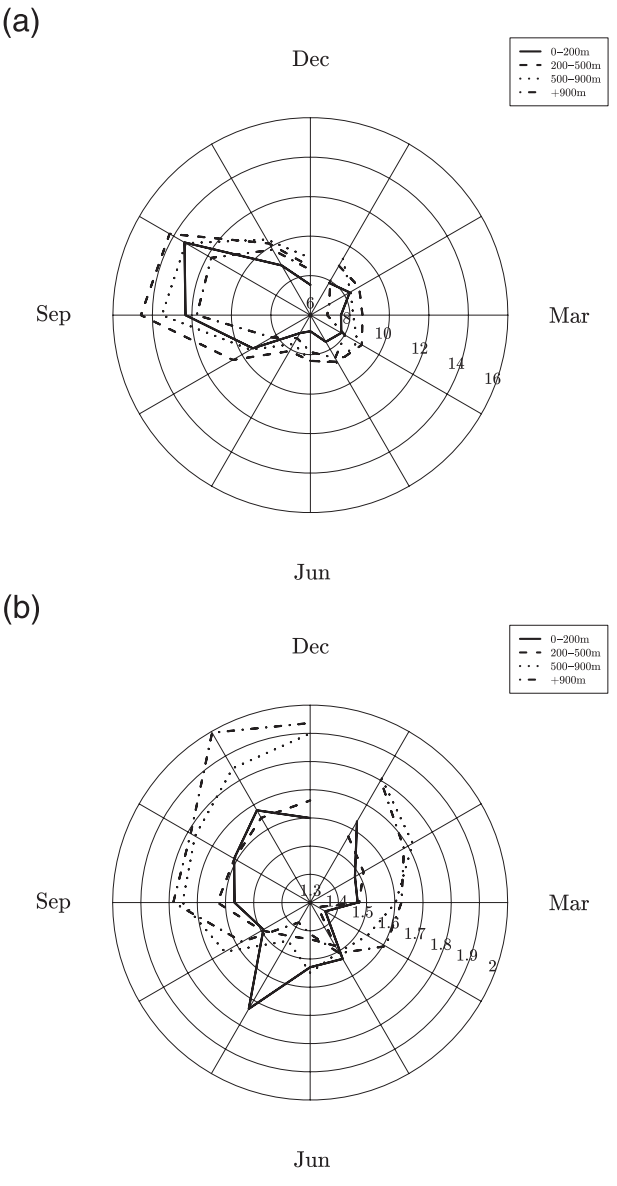


FIG. 9. As in Fig. 9, but for daily intrinsic-rainfall intensity.

selected periods: the first is the month of July, the second spans September and October. We excluded months that can merge different regimes like June and August, which are at the transition between spring and summer or summer and fall. The medians of the point intensity have been kriged (appendix B) and mapped in Fig. 11. The analysis focuses first on the month of July (Figs. 11a,c). In July, the daily and hourly rainfall intensity patterns are similar as already suggested by Fig. 9. The maximum median intensities either at the daily or hourly durations are located about 100 km from the shoreline over the Baronnies, Alpine foothill on the east side of the Rhône River valley (the maximum over the Alps in Fig. 11a is not significant as indicated by the kriging variance, not shown). The median intensity patterns show two main gradients, one south–north along the Mediterranean shore and one west–east. The rainfall intensity increases by a factor of 2 at the hourly time step (Fig. 11c) from the shore or the mountain ridge to location of the maximum (from 0.7 to 1.4 mm $h^{-1}$), while the daily rainfall intensity varies of about 20% (from 7 to 9 mm $day^{-1}$). During the September–October period, the pattern of the hourly median intensity (Fig. 11d) is also similar to the pattern for July. The maximum median intensity is equal to the one in July (Fig. 11c), the west–east gradient is similar in intensity to the one in July but the south–north gradient is lower.

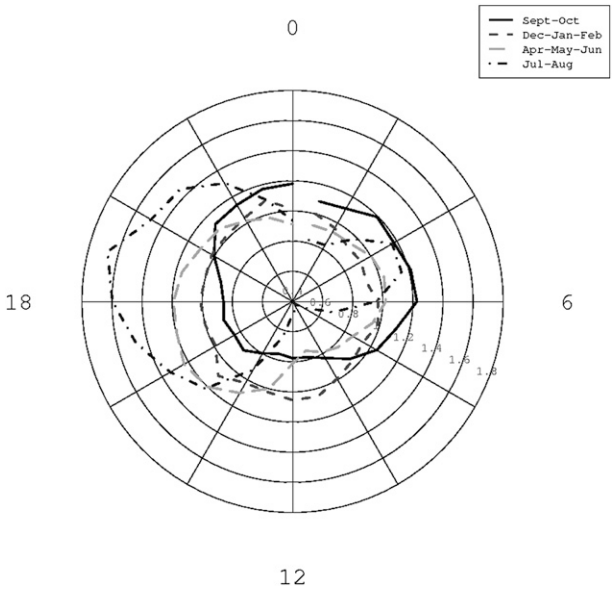


FIG. 10. Diurnal cycle of the normalized hourly intrinsic-rainfall intensity for months of September–October (solid), December–February (short black dashes), April–June (long gray dashes), and July–August (dashed–dotted). The indicated times are in UTC, which is close to the local time in the study region.

The rainfall intensity along the shore increases from July to September–October at the hourly duration. The daily rainfall intensity map of September–October (Fig. 11b) contrasts a lot with the one in July. The median intensity is lower by a factor of 3 or 4, which means that lighter rainfall is included in the distribution and furthermore the pattern is far more different. The maximum median values of September–October are over the Cévennes Mountain while it was along the Rhône River valley in July.

### *c. Spatial structure of rainfall events*

To gain further insight about the difference between the rainfall events occurring over the plain or over the mountain for the spring, summer, or fall seasons, we have calculated the climatological variogram (Bastin et al. 1984) of the rainfall residuals to the median intensity associated with rainy events. The climatological variogram takes benefits of the large amount of data gathered in each sample set and provide a bulk estimate of the structure of each rainy-event population. To distinguish the different statistical populations, the datasets are disjoints in space and time. Datasets gather either rain gauge data from altitudes lower than 200 m or higher than 500 m, and as explained before the events of a dataset come from the central month of the seasons: April, July, and October. The climatological variograms are plotted in Fig. 12a–c, and Fig. 12d shows the number of pairs used to compute each average variogram. Each variogram increases monotonically with the distance up to a sill of around 1, indicating that the variograms of each individual rainfall fields tend on average to the field variance. We emphasize that the variograms are computed on normalized residuals. Working on residuals removes the nonstationary component of the rainfall field illustrated in Fig. 11. The normalization allows one to mix nonsynchronous rainfall fields belonging to the same population. Such random fields are called second-order stationary random functions as the two first moments of their distribution, that is, the mean and the covariance, are defined (Chiles and Delfiner 1999). In this case, the spatial structure of the rainfall events is well defined and their size is characterized by the range (so-called decorrelation distance).

Whatever the elevation, the distances of the July rainfall fields are the shortest being about 20–30 km. In October above 500 m, the decorrelation distance is only 10 km larger (30–40 km), while it increases sensibly to 50–60 km below 200-m altitude and in April for any altitude.

Theoretically, the variogram is equal to zero at the origin. A difference between the experimental and the theoretical variogram at the origin is called a nugget effect and reveals either variability at very short distance or measurement errors. With an average distance between hourly rain gauges higher than 8 km, the observed nugget effect is probably due to the small-scale variability of the rainfall field.

The climatological variograms appear to be very similar for the events occurring anywhere in July, while in April and October the mountainous and plain events have very different structures.

## 6. Maximum rainfall intensity

Maximum rainfall intensities are also important to investigate rainfall regimes. We first examine the month of occurrence of maximum rainfall intensities. Rain gauge stations are gathered into the four altitude ranges used to analyze rainfall accumulation, intermittency and regular intensity in sections 3 and 4. Each year, the month of occurrence of the maximum rainfall intensity is determined in each of the four altitude ranges. This is a set of 16 and 43 values for the occurrences of, respectively, the hourly (1993–2008) and daily (1958–2000) maximums. The histograms of these two random variables are plotted in Fig. 13. Almost all the hourly maximums occur in between July and September, August being the mode with 50% of the occurrences. The month of occurrence is independent of the altitude. This is not the case for the daily maximums (Fig. 13b). Below 500 m of altitude, the daily maximums

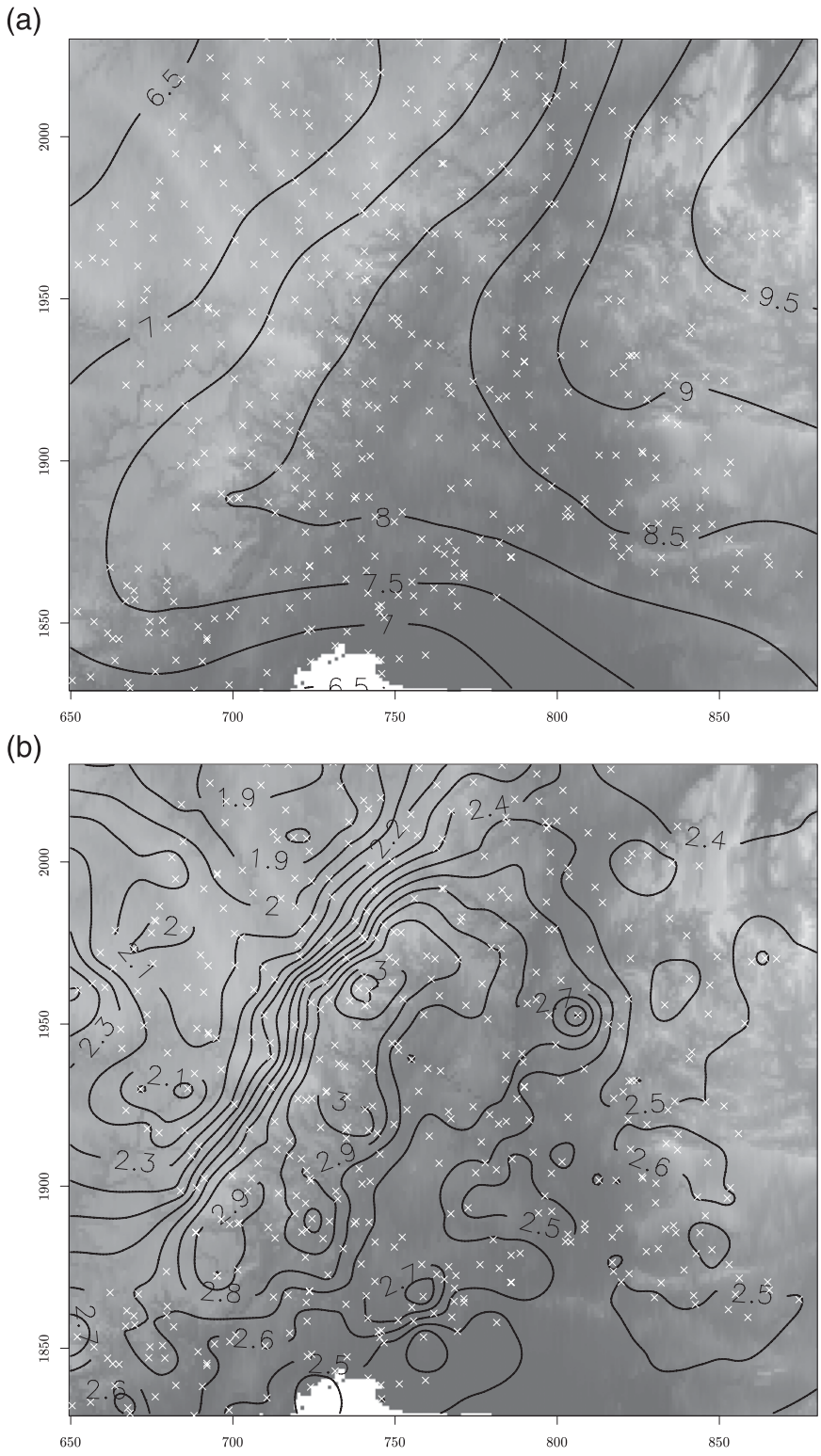


FIG. 11. (a) Median of the July daily intrinsic-rainfall intensity. (b) As in (a), but for September and October. (c),(d) As in (a),(b), but for the hourly intensity.

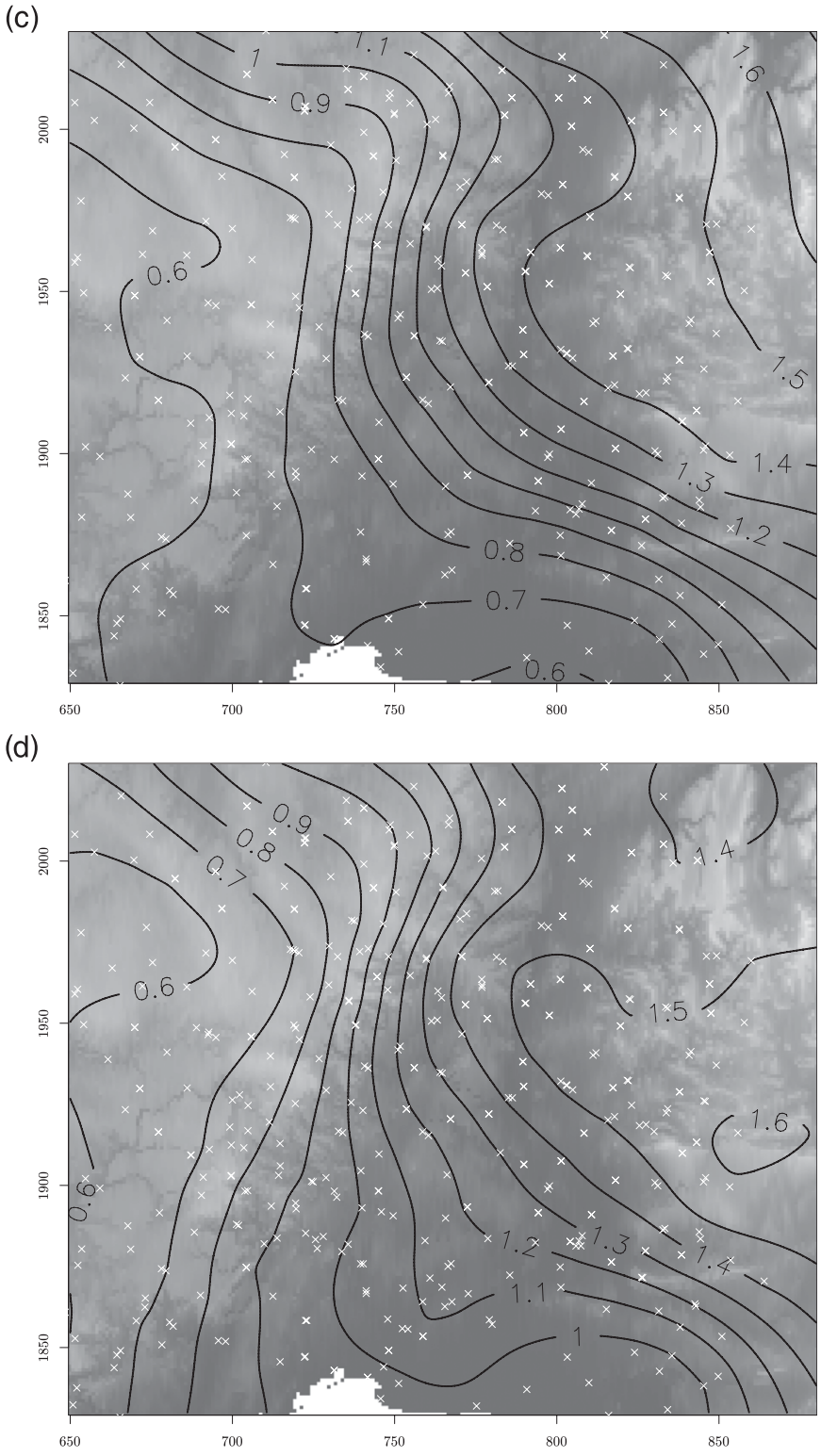


FIG. 11. (*Continued*)

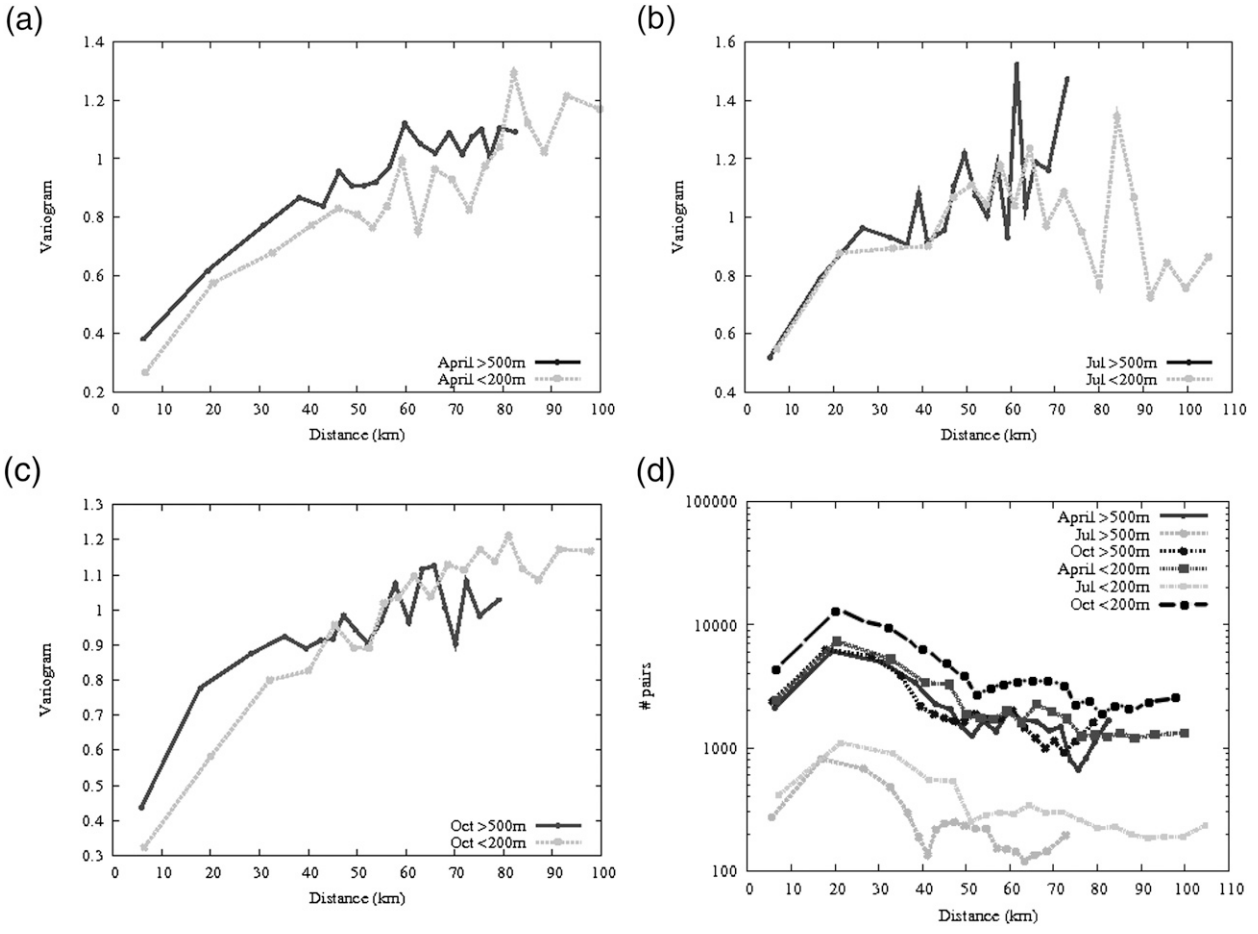


FIG. 12. Climatological variograms of the intrinsic-rainfall intensity during rainfall events for rain gauges above (solid curve) and below (dashed–dotted curve plus filled circle) 250-m altitude for (a) April, (b) July, and (c) October. (d) Number of rain gauge couples used for the variogram computation.

occur quasi exclusively in August and September; above 500 m, they are almost equivalently distributed from August to November.

Maximum rainfall intensities are usually characterized by their return period (inverse of the frequency of exceedance). The shortness of rainfall series and the complex topography of the study region make difficult the identification of an ad hoc maximum rainfall density function (Ceresetti et al. 2010). The procedure implemented in this paper consists of collecting one maximum value a year for the daily and the hourly databases and to analyze the median of their distribution. Figure 14a shows that for hourly maxima the locations of the highest medians are over the southern part of the Cévennes foothill near the town of Alès. This location is very different from the highest medians of the regular rainfall intensities that are over the Baronnies (Fig. 11a). We note a difference of a factor of 10 between the median of the maximums and the maximum of the median intensities. Such a difference confirms the widespread of the hourly intensity distributions. The same remark holds for daily intensities even though the scale transform of distributions with duration may be more complex than suggested (Ceresetti et al. 2010; Venugopal et al. 2006; among others). Unlike the hourly duration, the highest daily maxima are located over the Serres de la Croix de Bauzon massif like the maximum of the intensity medians (Fig. 11b).

The top 10 maximum hourly and daily intensities are given, respectively, in Tables 3 and 4 and plotted on the maps of the maximum rainfall intensity medians (Fig. 14). The top 10 hourly maximums look randomly located while the daily maximums are clustered into two groups collocated with the highest intensity medians. One is located over the southern slope of the Cévennes massif, the second along the mountain ridge in between the Mont Lozere (highest summit of the Cévennes) and the Serre de la Croix de Bauzon.

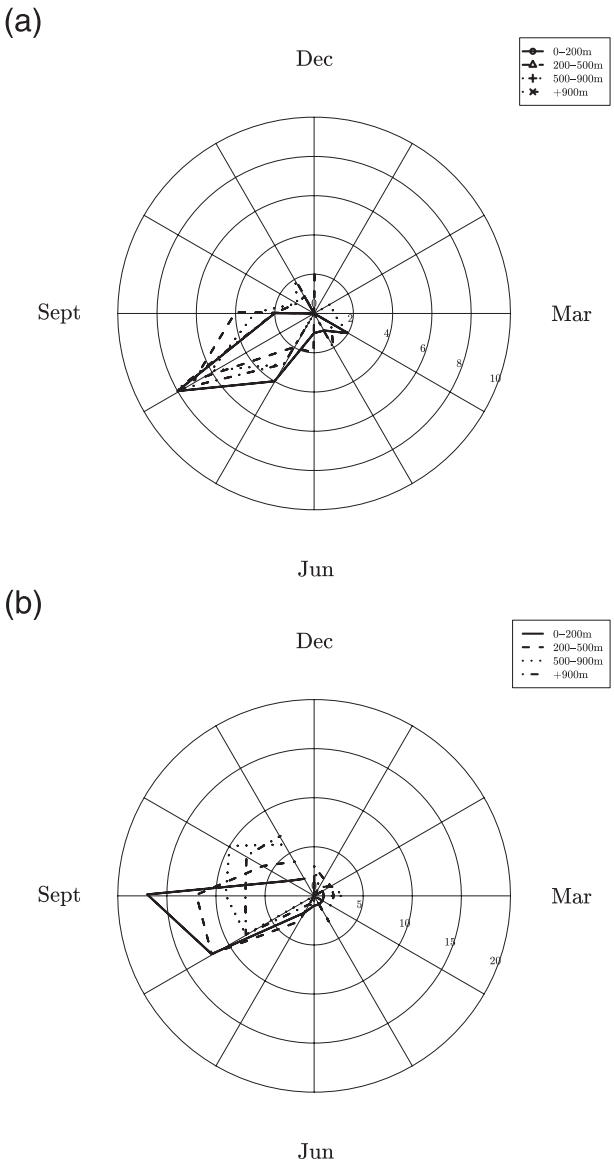


FIG. 13. Monthly histograms of (a) hourly and (b) daily maximum rainfall intensities in four altitude ranges.

## 7. Signature of some underlying meteorological processes

The purpose of this section is to discuss different features of the rainfall regime in the light of meteorological processes reported in the literature. This discussion is biased toward the situations producing heavy precipitations that have been studied in more details in relation to floods. Basically, as in many temperate areas, three types of meteorological processes lead to rain production in this region, covering the all range of mesoscales proposed by Orlanski (1975): airmass convection producing local thunderstorms ($\alpha$ mesoscale), organized convection producing severe multicell storms ($\beta$ mesoscale), and extratropical cyclones producing frontal rain ($\gamma$ mesoscale). Given the marked topography of the region, orographic effects are also present, probably interacting with the above processes.

Airmass thunderstorms mainly occur during the summer. They occur in low wind shear environments, typically last one hour, and have a marked diurnal cycle with a maximum of occurrence in the late afternoon (Chappell 1987; S. Coquillat and E. Defer 2010, personal communication; Oriol 2008; Dai 2001; Dai et al. 1999; Molinié et al. 1999).

The signature of airmass storms in the summer rainfall regime is imprinted in (i) the intermittency, which indicates that storms last one hour or less (Fig. 6a); (ii) in the hourly and daily intensities, which are similar at low altitude (Figs. 8 and 9); (iii) in rainfall patterns that are similar in size to this of airmass storms (variogram range of the hourly intensity of about 20–30 km, Fig. 12) and on the diurnal cycle of the intensity, which peaks in the late afternoon in July (Fig. 10).

Frontal rain may occur at all seasons with a clear minimum of occurrence during the summer season when low pressure circulation over the northern Atlantic Ocean moves north. Frontal rain feature typical durations in days, widespread distribution in space, low intermittency, and weak to moderate intensities. They are expected to produce more rain on west-facing slopes, namely on the Baronnies. Their signature might be imprinted on the map of the median daily intensity on the left side of the Rhône River (Fig. 11b) even though it is difficult to identify because of the predominance of the others meteorological processes producing rain.

Mesoscale convective systems are generally embedded in the warm sector of extratropical cyclones during the spring and even more often during the fall season. They produce severe multicell storms lasting several hours possibly at the same place (see different event analyses in Sénési et al. 1996; Ducrocq et al. 2002, 2003; Delrieu et al. 2005; Nuissier et al. 2008). In France, those situations are called ''episodes cévenols'' according to the name of the west part of the study area. They have been extensively studied because they yield HPEs and in turn severe flash-flooding conditions. Different numerical modeling studies demonstrated their intrinsic mechanisms that require low-level inflows of warm and humid air (Ducrocq et al. 2008; Lebeaupin et al. 2006) as well as their predictability (Anquetin et al. 2005).

As a consequence of the specific features of mesoscale convective systems (MCSs), the rainfall regime of the fall season (and of the spring one to a lesser extent) is marked by the singular characteristics of these events: (i) locations of the maximum medians of the hourly

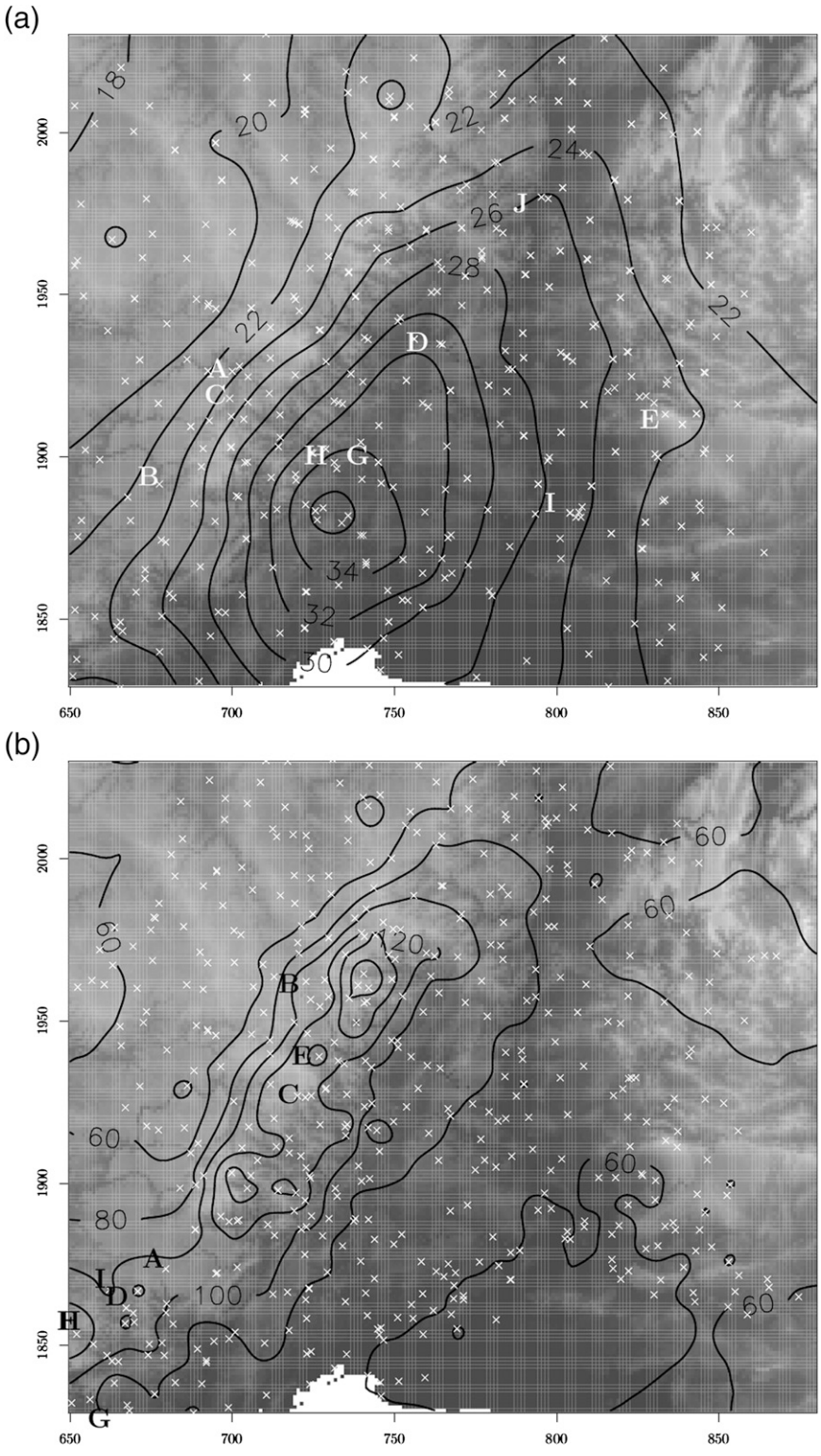


FIG. 14. Median (a) hourly and (b) daily annual maximum rainfall intensities (isocontours). The letters A–I are the indices of the top 10 rainfall maximums at either the hourly or the daily durations as referred to in Tables 3 and 4. The background topography is similar to Fig. 1b.

TABLE 3. Top 10 maximum hourly rainfall intensities during the 1989–2008 period. XLIIE and YLIIE are the Lambert II extended Cartesian coordinates of the rain gauge stations.

| Index | XLIIE | YLIIE | Alt | Date (UTC) | Rainfall intensity (mm $h^{-1}$) |
|---|---|---|---|---|---|
| A | 700.0 | 1926.3 | 549 | 1400 27 Dec 2006 | 240.6 |
| B | 677.5 | 1891.5 | 492 | 1400 27 Dec 2006 | 230.3 |
| C | 699.2 | 1918.0 | 665 | 1400 27 Dec 2006 | 180.3 |
| D | 748.7 | 2011.2 | 1180 | 1000 1 Oct 2007 | 175 |
| E | 764.0 | 1934.9 | 127 | 1600 8 Sep 2005 | 158 |
| F | 838.7 | 1909.9 | 1455 | 0500 29 Dec 1996 | 154.5 |
| G | 652.6 | 1750.4 | 7 | 0100 25 Aug 2002 | 117 |
| H | 745.0 | 1898.3 | 183 | 1500 22 Sep 1993 | 116 |
| I | 731.4 | 1898.2 | 139 | 0200 9 Sep 2002 | 107.9 |
| J | 806.9 | 1882.9 | 110 | 0200 2 Jul 1996 | 103.1 |

TABLE 4. As in Table 3 but for the daily intensities.

| Index | XLIIE | YLIIE | Alt | Date (UTC) | Rainfall intensity (mm $day^{-1}$) |
|---|---|---|---|---|---|
| A | 679.5 | 1873.6 | 730 | 0700 21 Sep 1992 | 447.6 |
| B | 722.7 | 1962.2 | 980 | 0700 1 Nov 1968 | 437 |
| C | 722.5 | 1926.9 | 1000 | 0700 7 Nov 1982 | 350 |
| D | 667.2 | 1861.6 | 435 | 0700 4 Nov 1997 | 347.8 |
| E | 726.7 | 1939.1 | 620 | 0700 20 Sep 1980 | 344 |
| F | 726.7 | 1939.1 | 620 | 0700 7 Nov 1982 | 337.6 |
| G | 652.0 | 1853.5 | 620 | 0700 4 Nov 1997 | 336 |
| H | 661.9 | 1821.9 | 90 | 0700 26 Sep 1992 | 312.2 |
| I | 652.0 | 1853.5 | 620 | 0700 16 Dec 1995 | 305 |
| J | 662.1 | 1867.2 | 435 | 0700 20 Sep 1980 | 304 |

intrinsic intensities are mapped where the MCSs are expected to form in the Rhône Valley (Fig. 11d); (ii) the decorrelation distance of rainfall patterns is higher than for isolated convection because of both the size of the clusters of moving rainfall cells and the advection of the MCS itself (Berne et al. 2004); (iii) the convective cells embedded in MCSs are triggered during the night (Fig. 10).

Orography seemingly influences the different rainfall production mechanisms across the range of scales seen above. Recent studies over western Mediterranean regions showed that the different scales of a relief trigger different scales of convection. On the one hand, the presence and shape of the mountain chains themselves modify the mesoscale circulation in a way that determines the triggering of MCSs as well as its positioning, most generally upstream the mountain ridge (Chu and Lin 2000; Rotunno and Ferretti 2001; Ducrocq et al. 2008). On the other hand, the small details of the topography, basically mounts and valleys, trigger shallow convection organized in bands that develop downstream and can last as long as a low-level jet of moist air persists upstream (Miniscloux et al. 2001; Anquetin et al. 2003; Kirshbaum and Durran 2004; Kirshbaum et al. 2007). Even if they have comparable typical durations, orographic banded convection displays rainfall features radically different from MCS. The rainfall intensities are small at small time steps (from 10 to 30 mm $h^{-1}$) but heavy at large time steps (200 mm $day^{-1}$) because they are continuous in time. As shown in Godart et al. (2011), orographic rainbands supply almost 40% of the fall rain amount. The rainfall patterns cover the mountain ridge and the size, spacing and orientation of the bands are related to both topography and upstream flow conditions.

In relation with the role of topography various features of the rainfall regime can be explained. (i) The median pattern of the daily intrinsic intensity slightly varies from summer to fall (Figs. 11a,b). The rainfall lasts on average 10% of the day (2.5 h), which is 2.5 times more than for summer events (Fig. 6a). (ii) In consequence of the size of the respective systems, the mean variogram range over the shallow convective area is of only 30–40 km, while the MCS rainfall occurring over the valley during the same season doubles the average range (60–70 km) (Fig. 12). (iii) The highest daily maximums (Fig. 14b) and the highest daily intensities (Fig. 11b) are collocated along the three higher mountains of the Cévennes massif: Mont Aigoual, Mont Lozère, and Serre de la Croix de Beauzon, which is different from what is observed for hourly data when the intensity of the orographic banded convection is much lower.

## 8. Conclusions

This study describes the rainfall regime in a Mediterranean region of the southeast of France from hourly to annual time scales. The region is exposed to both oceanic and Mediterranean influence. The terrain of the region is partly mountainous and plays a major role on rainfall properties. The analysis relies on basic statistics of point variables such as rainfall accumulation, intermittency, and nonzero intensity. The study makes a distinction between regular and extreme rainfall, although others studies are more insightful concerning extreme rainfall in the region (Ceresetti et al. 2010; Bois et al. 1997). The use of geostatistics allows depicting the spatial patterns of different rainfall properties despite their non-first-order stationarity.

The rainfall regime of the study region appears significantly contrasted from many points of view. The average yearly rainfall accumulation runs from 0.5 m over the plain to more than 2.0 m over the mountain range. The rain–no-rain intermittency undergoes also large variations in time and space. For example, it rains about 7 days

a month at altitudes below 200 m MSL and 13 days above 900 m MSL. Considering the event intermittency, the results are similar, and the length of the rainy periods during wet days increases with the altitude. The relief seems also to be among the main governing factors of rainfall intensity. However, this last property requires an analysis at different temporal scale (hourly and daily) and to distinguish between regular and extreme rainfall events. At the hourly resolution, the highest average rainfall intensities are inland along the Rhône Valley while hourly rainfall extremes switch to the southwest, closer to the Mediterranean Sea, over the Cévennes foothills. The locations of the highest daily rainfall intensities concerning both regular and extreme events are very different from the hourly ones: they are collocated over the Cévennes Mountain Range. A cross analysis of these rainfall properties at different time and space scales highlights the signature of some dominant atmospheric processes on rainfall patterns in time and space.

This study illustrates the great potential use of rain gauge networks to depict climatic features. Even if the space resolution is too coarse to analyze individual rainfall events, the climatological analysis is proven to be able to dissect rather precisely the areas of influence of the different governing meteorological processes. From a practical point of view, the main limitation of such networks is their evolution in time. With very good intentions, network managers improve their networks year after year, upgrading instruments and rationalizing their coverage. These evolutions introduce heterogeneities in series. They could be accounted for using sophisticated methods like error kriging, but nevertheless they introduce additional complexity in the analysis of the results and they prevent reliable detection of possible effects of the climate change.

*Acknowledgments.* Eddy Yates and Angélique Godart, Ph.D. students at LTHE, have yielded insightful statistics on the current topics. The authors have greatly appreciated their knowledge on the Cévennes–Vivarais rainfall regime and are grateful for fruitful discussions issued.

The authors acknowledge the French meteorological service Météo-France and the survey service OHMCV for providing the rainfall data of the study.

The authors are grateful to reviewers for their pertinent remarks and careful reading.

## APPENDIX A

### Variogram

Suppose $Z(\mathbf{x})$ is a random function depending on the space coordinate $\mathbf{x}$. Assuming the isotropy of the $Z$ structure, the variogram of $Z$ is defined for a separation distance $h$ by

$$\gamma(h) = \frac{1}{2}\mathrm{Var}[Z(x + h) - Z(x)]. \quad \text{(A1)}$$

Similarly to the covariance, the variogram is a structure function. One of the variogram advantages over the covariance is its independence on the mean of $Z$. In this paper, the estimate of the rainfall field variogram $\hat{\gamma}$ is the average of the experimental variogram computed as a function of the separation distance $h$:

$$\hat{\gamma}(h) = \frac{1}{2N(h)} \sum_{x_i - x_j = h} [Z(x_i) - Z(x_j)]^2, \quad \text{(A2)}$$

where $N(h)$ is the number of point pairs separated by a distance of $h$.

To estimate the variogram for nonsampled distances, a variogram model is fitted onto the average variogram. The model is the so-called spherical model defined as

$$\gamma(h) = \begin{cases} \mathrm{nug} + \mathrm{sil}\left(\dfrac{3}{2}\dfrac{h}{\mathrm{ran}} - \dfrac{1}{2}\dfrac{h^3}{\mathrm{ran}^3}\right) & \text{if} \quad 0 \le h \le \mathrm{ran} \\ \mathrm{nug} + \mathrm{sil} & \text{if} \quad h > \mathrm{ran} \end{cases}. \quad \text{(A3)}$$

1) The term nug is called the nugget effect and is defined by nug = $\gamma(0)$. A positive nugget effect indicates either a small-scale variability of the field or uncertainties on point measurements.
2) The term ran is the variogram range. For distances $h$ below the range, $\gamma(h)$ monotonically increases with $h$; beyond the range, $\gamma(h)$ is equal to the sill (sil).

## APPENDIX B

### Kriging

Kriging is a linear interpolation method particularly adapted to the interpolation of rain gauge measurements in the study region. If $Z(x)$ is a regionalized random function with $x$ representing the space or time coordinates, kriging provides an estimate $Z^*(x_0)$ of the random variable $Z(x_0)$ at the target point $x_0$, based on the measurements $Z(x_\alpha)$,

$$Z^*(x_0) = \sum_\alpha \lambda_\alpha Z(x_\alpha) + \lambda_0, \quad \text{(B1)}$$

with $\alpha$ an index of the data points, $\lambda_\alpha$ the interpolation weights, and $\lambda_0$ a constant. The interpolation coefficients

$\lambda_\alpha$ and $\lambda_0$ are computed by using a constraint on the nonbias of the estimator $\{E[Z^*(x_0) - Z(x_0)] = 0\}$ and another on the minimization of the estimation variance $\{\mathrm{Var}[Z^*(x_0) - Z(x_0)]\} = 0$. It is shown in literature that the interpolation weights depend of the $Z(x)$ variogram. Among the interesting properties of kriging are the following:

- The estimation variance can be expressed as a function of the variogram.
- Kriging is an exact interpolator. In the real world, this condition is met only in the case of a zero variogram nugget.
- At any point $x_0$ featuring a distance from any measurement beyond the variogram range, the estimator $Z^*(x_0)$ is equal to the average of the data $Z(x_\alpha)$.
- The estimated field is smoother than the actual one.

## REFERENCES


Alpert, P., 1986: Mesoscale indexing of the distribution of orographic precipitation over high mountains. *J. Climate Appl. Meteor.,* **25,** 532–545.

——, and H. Shafir, 1989: Meso $\gamma$-scale distribution of orographic precipitation: Numerical study and comparison with precipitation derived from radar measurements. *J. Appl. Meteor.,* **28,** 1105–1117.

Anquetin, S., F. Minsicloux, J.-D. Creutin, and S. Cosma, 2003: Numerical simulation of orographic rainbands. *J. Geophys. Res.,* **108,** 8386, doi:10.1029/2002JD001593.

——, and Coauthors, 2005: The 8 and 9 September 2002 flash flood event in France: A model intercomparison. *Nat. Hazards Earth Syst. Sci.,* **5,** 741–754.

——, E. Yates, and V. Mano, 2006: Sensitivity of orographic precipitation to changing soil moisture and ambient conditions. Preprints, *12th Conf. on Mountain Meteorology,* Santa Fe, NM, Amer. Meteor. Soc., 2.2. [Available online at http://ams.confex.com/ams/SantaFe2006/techprogram/paper_114069.htm.]

Antoine, J., B. Desailly, and F. Gazelle, 2001: Les crues meurtrières, du Roussillon aux Cévennes. *Ann. Geogr.,* **110,** 597–623.

Barancourt, C., J.-D. Creutin, and J. Rivoirard, 1992: A method for delineating and estimating rainfall fields. *Water Resour. Res.,* **28,** 1133–1143.

Barnet, D. N., S. J. Brown, J. Murphy, D. M. H. Sexton, and M. Webb, 2006: Quantifying uncertainty in changes in extreme event frequency in response to doubled $CO_2$ using a large ensemble of CGM simulations. *Climate Dyn.,* **26,** 489–511.

Bastin, G., B. Lorent, and M. Gevers, 1984: Optimal estimation of the average rainfall and optimal selection of rain gauge locations. *Water Resour. Res.,* **20,** 463–470.

Berne, A., G. Delrieu, J. Creutin, and C. Obled, 2004: Temporal and spatial resolution of rainfall measurements required for urban hydrology. *J. Hydrol.,* **299,** 166–170.

Bois, P., H. Mailloux, C. Obled, and F. De Saintignon, 1997: Atlas expérimental des risques de pluies intenses dans la région Cévennes-Vivarais. Tech. Rep., Pôle Grenoblois des Risques Naturels, LAMA, 17 pp.

Bolle, H., 2003: Climate, climate variability, and impacts in the Mediterranean area: An overview. *Mediterranean Climate: Variability and Trends,* Springer, 1–81.

Braud, I., J.-D. Creutin, and C. Barancourt, 1993: The relation between the mean areal rainfall and the fractional area where it rains above a given threshold. *J. Appl. Meteor.,* **32,** 193–202.

Ceresetti, D., G. Molinié, and J.-D. Creutin, 2010: Scaling properties of heavy rainfall at short duration: A regional analysis. *Water Resour. Res.,* **46,** W09531, doi:10.1029/2009WR008603.

——, S. Anquetin, G. Molinié, E. Leblois, and J. Creutin, 2012: Multiscale evaluation of extreme rainfall event predictions using severity diagrams. *Wea. Forecasting,* **27,** 174–188.

Chappell, C. F., 1987: Quasi-stationary convective events. *Mesoscale Meteorology and Forecasting,* P. S. Ray., Ed., Amer. Meteor. Soc., 289–310.

Chiles, J.-P., and P. Delfiner, 1999: *Geostatistics: Modeling Spatial Uncertainty*. Wiley and Sons, 720 pp.

Chu, C.-M., and Y.-L. Lin, 2000: Effects of orography on the generation and propagation of mesoscale convective systems in a two-dimensional conditionally unstable flow. *J. Atmos. Sci.,* **57,** 3817–3837.

Dai, A., 2001: Global precipitation and thunderstorm frequencies. Part II: Diurnal variations. *J. Climate,* **14,** 1112–1128.

——, F. Giorgi, and K. E. Trenberth, 1999: Observed and model-simulated diurnal cycles of precipitation over the contiguous United States. *J. Geophys. Res.,* **104** (D6), 6377–6402.

Delrieu, G., 2003: L'Observatoire Hydro-météorologique Méditerranéen Cévennes–Vivarais (the Cévennes–Vivarais Mediterranean Hydrometeorological Observatory). *La Houille Blanche,* **6,** 83–88.

——, and Coauthors, 2005: The catastrophic flash-flood event of 8–9 September 2002 in the Gard region, France: A first case study for the Cévennes–Vivarais Mediterranean Hydrometeorological Observatory. *J. Hydrometeor.,* **6,** 34–52.

de Montera, L., L. Barthés, C. Mallet, and P. Golé, 2009: The effect of rain–no rain intermittency on the estimation of the universal multifractals model parameters. *J. Hydrometeor.,* **10,** 493–506.

Ducrocq, V., D. Ricard, J. Lafore, and F. Orain, 2002: Storm-scale numerical rainfall prediction for five precipitating events over France: On the importance of the initial humidity field. *Wea. Forecasting,* **17,** 1236–1256.

——, G. Aullo, and P. Santurette, 2003: Les précipitations intenses et les inondations des 12 et 13 Novembre 1999 sur le sud de la France. *Meteorologie,* **42,** 18–27.

——, O. Nuissier, D. Ricard, C. Lebeaupin, and T. Thouvenin, 2008: A numerical study of three catastrophic precipitating events over southern France. II: Mesoscale triggering and stationarity factors. *Quart. J. Roy. Meteor. Soc.,* **134,** 131–145.

Frei, C., and C. Schär, 1998: A precipitation climatology of the Alps from high-resolution rain-gauge observations. *Int. J. Climatol.,* **18,** 873–900.

Giorgi, F., 2006: Climate change hot-spots. *Geophys. Res. Lett.,* **33,** L08707, doi:10.1029/2006GL025734.

Godart, A., S. Anquetin, and E. Leblois, 2009: Rainfall regimes associated with banded convection in the Cévennes–Vivarais area. *Meteor. Atmos. Phys.,* **103** (1–4), 25–34, doi:10.1007/s00703-008-0326-3.

——, ——, ——, and J. Creutin, 2011: The contribution of orographically driven banded precipitation to the rainfall climatology of a Mediterranean region. *J. Appl. Meteor. Climatol.,* **50,** 2235–2246.

Jacq, V., 1994: Inventaire des situations à précipitations diliviennes sur les régions Languedoc-Roussillon, PACA et Corse, période 1958–1994 (Inventory of extreme precipitation events in the Languedoc-Roussillon, PACA and Corse regions in the period 1958–2004). Phénomènes remarquables, Tech. Rep. 3, Météo-France (SCEM), 190 pp.

Johnson, G. L., and C. L. Hanson, 1995: Topographic and atmospheric influences on precipitation variability over a mountainous watershed. *J. Appl. Meteor.,* **34,** 68–86.

Kirshbaum, D. J., and D. Durran, 2004: Factors governing cellular convection in orographic precipitation. *J. Atmos. Sci.,* **61,** 682–698.

——, G. Bryan, R. Rotunno, and D. Durran, 2007: The triggering of orographic rainbands by small scale topography. *J. Atmos. Sci.,* **64,** 4222–4245.

Lebeaupin, C., V. Ducrocq, and H. Giordani, 2006: Sensitivity of torrential rain events to the sea surface temperature based on high-resolution numerical forecasts. *J. Geophys. Res.,* **111,** D12110, doi:10.1029/2005JD006541.

Lebel, T., and G. Bastin, 1985: Variogram identification by the mean-squared interpolation error method with application to hydrologic fields. *J. Hydrol.,* **77,** 31–56.

Michaud, J., B. Auvine, and O. C. Penalba, 1995: Spatial and elevation variations of summer rainfall in the southwestern United States. *J. Appl. Meteor.,* **34,** 2689–2703.

Miniscloux, F., J. D. Creutin, and S. Anquetin, 2001: Geostatistical analysis of orographic rainbands. *J. Appl. Meteor.,* **40,** 1835–1854.

Molini, A., G. G. Katul, and A. Porporato, 2010: Causality across rainfall time scales revealed by continuous wavelet transforms. *J. Geophys. Res.,* **115,** D14123, doi:10.1029/2009JD013016.

Molinié, G., S. Soula, and S. Chauzy, 1999: Cloud-to-ground lightning activity and radar observations of storms in the Pyrénées range area. *Quart. J. Roy. Meteor. Soc.,* **125,** 3103–3122.

Nuissier, O., V. Ducrocq, D. Ricard, C. Lebeaupin, and S. Anquetin, 2008: A numerical study of three catastrophic precipitating events over southern France. I: Numerical framework and synoptic ingredients. *Quart. J. Roy. Meteor. Soc.,* **134,** 111–130.

——, B. Joly, A. Joly, V. Ducrocq, and P. Arbogast, 2011: A statistical downscaling to identify the large scale circulation patterns associated with heavy precipitation events over southern France. *Quart. J. Roy. Meteor. Soc.,* **137,** 1812–1827.

Oriol, R., 2008: Etude des éclairs en région Cévennes–Vivarais: Apport pour l'identification des types de pluies. M.S. thesis, Université Joseph Fourier, Observatoire des Sciences de l'Univers de Grenoble, 28 pp.

Orlanski, I., 1975: A rational subdivision of scales for atmospheric processes. *Bull. Amer. Meteor. Soc.,* **56,** 527–530.

Peel, M. C., B. L. Finlayson, and T. A. Mc Mahon, 2007: Updated world map of the Köppen-Geiger climate classification. *Hydrol. Earth Syst. Sci.,* **11,** 1633–1644.

Pidwirny, M., cited 2011: Climate classification and climatic regions of the world. *Fundamentals of Physical Geography,* 2nd ed. [Available online at http://www.physicalgeography.net/fundamentals/7v.html.]

Ricard, D., 2002: Initialisation et assimilation de données à mésoéchelle pour la prévision à haute résolution des pluies intenses de la région Cévennes–Vivarais (in French). Ph.D. thesis, Université Paul Sabatier-Toulouse III, 250 pp.

——, V. Ducrocq, and L. Auger, 2011: A climatology of the mesoscale environment associated with heavily precipitating events over a northwestern Mediterranean area. *J. Appl. Meteor. Climatol.,* **51,** 468–488.

Rotunno, R., and R. Ferretti, 2001: Mechanisms of intense alpine rainfall. *J. Atmos. Sci.,* **58,** 1732–1749.

——, and R. A. Houze, 2007: Lessons on orographic precipitation from the mesoscale alpine programme. *Quart. J. Roy. Meteor. Soc.,* **133,** 811–830.

Sénési, S., P. Bougeault, J. Chèze, P. Cosentino, and R. Thepenier, 1996: The Vaison-la-Romaine flash flood: Mesoscale analysis and predictability issues. *Wea. Forecasting,* **11,** 417–442.

Venugopal, V., S. G., Roux, E. Foufoula-Georgiou, and A. Arneodo, 2006: Revisiting multifractality of high-resolution temporal rainfall using a wavelet-based formalism. *Water Resour. Res.,* **42,** W06D14, doi:10.1029/2005WR004489.

Yates, E., 2006: Convection en région Cévennes–Vivarais: Etude de données pluviométriques, simulations numériques et validation multi-échelles. Ph.D. thesis, ENSHMG, INP, 256 pp.